Karimi, N., Heeger, C., Christodoulou, L., and Dreizler, A. (2015) Experimental and theoretical investigation of the flashback of a swirling, bluff-body stabilised, premixed flame. Zeitschrift für Physikalische Chemie, 229(5), pp. 663-689.

Copyright © 2015 Walter de Gruyter GmbH.

A copy can be downloaded for personal non-commercial research or study, without prior permission or charge

The content must not be changed in any way or reproduced in any format or medium without the formal permission of the copyright holder(s)

When referring to this work, full bibliographic details must be given

http://eprints.gla.ac.uk/10073/

Deposited on: 15 May 2015

Enlighten – Research publications by members of the University of Glasgow http://eprints.gla.ac.uk

Experimental and theoretical investigation of the flashback of a swirling, bluff-body stabilised, premixed flame

Nader Karimi[1*], Christoph Heeger[2], Loizos Christodoulou[1], Andreas Dreizler[2]

[1]School of Engineering, University of Glasgow, G12 8QQ Glasgow, United Kingdom

[2]Institute of Reactive Flows and Diagnostics, Technische Universität Darmstadt, Darmstadt, Germany

Abstract

Flashback of an open turbulent, premixed flame in a swirl burner with central bluff-body is considered. The aim is to obtain further understanding of the physical mechanisms responsible for the upstream flame propagation. Previous studies on the same configuration hypothesised that there is an adverse pressure gradient in the direction of flame propagation. In this paper this is further investigated experimentally and theoretically. Static gauge pressure is measured on the surface of the bluff-body during flame flashback. Simultaneously, flame luminosity is imaged at 5 kHz. The results indicate that the static pressure rises downstream of the propagating reactive front. This is, then, discussed in the context of the theory of vortex bursting. An existing theory of flame propagation in the core flow is extended to a configuration similar to that investigated experimentally. The theory, although highly simplified, explains the generation of adverse pressure gradient across the flame and is qualitatively consistent with the experiment.

Introduction

Increasing concerns about the emission of nitrogen oxides has encouraged power industry to utilise lean premixed combustion in land-based power generation [1]. This combustion technology, although efficient in reducing NOx emission, suffers from a range of dynamic problems including thermoacoustic instabilities [2], flame flashback and blow-off [1]. Such issues severely limit the operability of the combustor and therefore have hindered the wide application of lean premixed combustion [3]. Amongst these, flame flashback is of particular significance. This is, in part, due to the fact that occurrence of flame flashback can seriously damage the combustor. Further, avoiding flame flashback remains a major challenge in the development of future hydrogen combustors and is therefore a key step in this area.

Flame flashback is usually regarded as the unwanted upstream propagation of a premixed/partially premixed flame. As a result of flashback, the flame may be stabilise in the mixing section of the burner upstream of its initial stabilisation point [4]. In practice, this can cause significant damage to the burner hardware and interrupt the operation. Thus flame flashback must be avoided. Lewis and von Elbe [5] proposed an early physical mechanism for this phenomenon. They related flashback to the retardation of the flow in the boundary layer and quenching of the flame through heat losses to the wall. This classical view, however, contradicted many

* Correspondence author (Nader.Karimi@glasgow.ac.uk)

experimental observations in real combustors [6, 7] and the problem remained mostly unexplained for a relatively long time.

Flame flashback is a transient phenomenon and happens in a short time (small fraction of a second) and is therefore difficult to study experimentally. Furthermore, it features highly stochastic and non-linear behaviours [4]. These are, perhaps, the reasons that up to recent years this subject, compared to the other areas of combustion dynamics, did not receive enough attention. The problem, however, has been recently revisited through employing advanced experimental and numerical techniques [4, 8-11]. Due to the wide application of swirling flows in gas turbines and industrial burners almost all recent studies of flashback considered this flow configuration. These efforts have led to the identification of the following mechanisms of flame flashback [4, 8]: flame propagation in boundary layer, flame propagation in the core of swirling flow, combustion instability induced flashback and flashback by combustion induced vortex breakdown. Here we briefly review each of these mechanisms.

Reduction of the flow velocity in the boundary layer promotes the upstream flame propagation [5]. On the other hand, heat and chemical species diffusion towards the wall tend to quench the flame [12-14]. It is argued that flame flashback is the ultimate result of a competition between these two effects [5]. In the literature, flame propagation in boundary layers is considered only pertinent to non-swirling low turbulent flames [8]. Thus, it is not usually regarded as a major mechanism of flashback in swirling flames [8]. However, it is not currently clear how significant this mechanism can be if it is combined with the other flashback mechanisms.

Flame flashback in swirling flows is closely related to the problem of flame propagation in a vortex axis. It is well documented that the flame propagation speed in vortices significantly increases compared to that in non-rotating flows [15, 16]. Ishizuka [17] has reviewed the proposed mechanisms of this flame propagation enhancement. Four main mechanisms were discussed by Ishizuka [17]. These include: flame kernel deformation, vortex bursting, baroclinic push and azimuthal vorticity evolution mechanism [17]. Flame kernel deformation is the direct consequence of centrifugal forces which tend to fling out the high density components and attract the lightest component to the rotation axis. Vortex bursting mechanism includes a rapid flame propagation supported by an aerodynamic force exerted on the flame [17]. This is due to the fact that lower density of combustion products weakens the centrifugal force close to the axis of rotation. Thus, it partially neutralises the low pressure caused by the circulation of the flow. This leads to the rise of static pressure across the flame and acts as a driving force which tends to push the flame inside the unburnt mixture [17, 18]. This is, of course, in clear contrast to flame propagation in non-rotating flows in which the static pressure decreases behind the flame. Such drop of the pressure is due the conversion of pressure into flow momentum downstream of a non-circulating premixed flame. On the other hand, rotation of the flow and the substantial density change by combustion produce an aerodynamic force which is exclusive to swirling flames [17, 18]. This is regarded as flame backpressure; Ishizuka [17] estimated this effect by the following relation

$$\Delta P = \rho_u V_{\theta}{}^2_{max} \left[1 - \left(\frac{\rho_b}{\rho_u}\right)^2\right]. \qquad (1)$$

In the above equation P, V and ρ are respectively pressure (Pa), velocity (m/s) and density (kg/m^3). Further, indices b, u and θ refer to the burnt, unburnt and tangential components. It has been argued in the literature [17, 18] that the total or partial conversion of this pressure difference to flow momentum generates a velocity field which facilitates upstream flame propagation. It should be noted, however, that the experimental validations of this pressure rise in swirling premixed flames are currently very limited [17].

A number of theoretical and experimental investigations have attempted to model the vortex bursting mechanism [19-23]. These works correlated the flame propagation speed to the maximum tangential velocity and density ratio of the burned and unburnt gases. Some of these models have been satisfactorily validated against the experiment [22]. Nonetheless, there are still some significant disagreements between the predictions of these models.

According to the vorticity transport equation the misalignment between the pressure and density gradients generates vorticity. It appears that this generation of vorticity can happen in swirling flames [24]. The induced negative axial velocity field can then promote the upstream flame propagation. The combustion products expand as a result of the combustion heat release and therefore the vortex grows in radius downstream of the flame. This expansion of the vortex tube activates two source terms of the vorticity transport equation, namely vorticity generation by the dilatation and vortex stretch [25, 26]. Azimuthal vorticity is generated on the shoulder of the flame and its induced velocity field convects the flame upstream. In a numerical simulation by Hasegawa et al. [27] it was shown that the baroclinic push is the dominant propagation mechanism shortly after the ignition. However, later the vortex stretch and dilatation overruled this mechanism [27]. In general, modelling of the above mentioned mechanisms revealed correlations between the flame propagation velocity and the maximum flow tangential velocity and density ratio [17-27]. These models assert that the flame propagation velocity increases in proportion to the vortex strength. However, there are still significant disparities between these correlations and not all of them are confirmed by experiment. This is perhaps an indication that the essential physics of flame and vortex interactions are not fully understood yet.

Thermoacoustic instabilities can generate large pressure waves in the combustor. This can result in reorganisation of the flow field and flashback of the flame, [28, 29]. It is well documented that premixed flames respond to acoustic excitation [2, 3, 30]. The extent of flame response depends substantially upon the flame and flow configurations and the characteristics of the acoustic excitation [2, 30]. In many cases the response is so strong that can cause hydrodynamic motion of the flame [28, 31]. It can further markedly modify the flow field through enhancing shear layer instabilities, vortex shedding and boundary layer separation [28, 30-33]. The modified combusting flow, in turn, feeds more energy into the acoustic waves and the instability grows [34]. Hence, it is not surprising that thermoacoustic instabilities may adversely influence flame stabilisation and cause flame flashback.

Many gas turbine and industrial combustors utilise aerodynamic flame stabilisation. This is achieved through swirling of the reactants and generating a recirculating bubble by the so called vortex breakdown [35]. This is a complicated fluid dynamic phenomenon which results in the breakdown of the vortical structures under certain conditions [35-37]. As a result of vortex breakdown, a region of low or negative velocity (i.e. a recirculation zone) is formed along the central axis of the swirling flow [35]. This can then anchor the flame [35]. Vortex breakdown has been subjected to extensive investigations in the context of aerodynamics [35-37]. Despite that, a comprehensive theory to explain the phenomenon has not merged yet [35]. It is known that there exist some flow features that can heavily affect the occurrence of vortex breakdown. These include introduction of positive pressure gradients and sudden flow expansion. These features exist in most swirling flames. Thus analogies have been proposed between the vortex breakdown in non-reacting flows and rapid flame propagation in vortex tubes [8]. In both cases a high pressure point along the axis of rotation brings the flow to stagnation and this is then followed by the formation of a recirculation zone [8].

The mechanism of vortex breakdown in combusting flows has been the subject of a number of investigations [8-11, 38, 39]. In an enclosed setup, flashback of a flame purely stabilised by vortex breakdown was studied experimentally and theoretically by Fritz et al. [8]. They showed that the swirling flow field broke down prior to flashback and allowed upstream propagation of the flame. The location of this breakdown in the reactive flow was further upstream compared to the corresponding isothermal flow. However, these authors [8] observed that this behaviour is highly dependent upon the combustor configuration and small design changes can prevent flashback. They, therefore, showed that a combusting flow can enhance the occurrence of vortex breakdown compared to its isothermal counterpart. Fritz et al. [8] explained this enhancement as the consequence of the pressure changes of the upstream flow due to the flame heat release. However, this remained as a phenomenological explanation and was not experimentally evaluated. These authors [8] then regarded this mechanism as Combustion Induced Vortex Breakdown (CIVB). In a flashback caused by this mechanism, the flame front propagates upstream of the retarded or reversed flow field generated by the CIVB [8]. Later Kiesewetter et al. [11] solved the vorticity transport equation numerically in a swirling flame using a two dimensional URANS code. They evaluated the influence of each source term in this equation on the flame upstream motion. Their analysis revealed that the baroclinic torque was the most significant contributor to the generation of negative axial velocity [11]. They argued that the ultimate stability of the flame was dependent upon a flame quenching process which occurred upstream of the flame [11]. The validity of this numerical simulation was confirmed through prediction of stability limits determined by the experiments of Fritz et al. [8]. Further experimental validation was performed by Konle et al. [10] through using high-speed PIV and LIF techniques.

In an attempt to understand the quenching of flashbacking flames, Kröner et al. [38] modelled turbulence and chemistry interactions in CIVB process. They considered the recirculation bubble ahead of the flame as a perfectly stirred reactor and proposed a burner specific time constant. This constant needed to be evaluated once experimentally for a specific burner configuration. The stability limits of the burner in various operating conditions could be then predicted by the model [38]. However, there was some systematic error in the model predictions [38]. Subsequently, this model was improved by Konle and Sattelmayer [39] and the assumption of perfectly stirred reactor was released for the low turbulent Reynolds numbers. This resulted in a better agreement of the model outputs with the experiment [39].

More recently, Heeger et al. [40] investigated flashback of a turbulent premixed flame in a swirl burner with central bluff-body. These authors used high speed laser diagnostics and produced time correlated data in the course of flame flashback. These included the velocity field of the unburnt gas through PIV, flame front detection by OH-PLIF and FL (Flame Luminosity) imaging [40]. Heeger et al. showed that in some flashback realisations there is a negative velocity region ahead of the flame which drives the flame upstream [40]. However, in a significant fraction of the total number of investigated flashbacks such a negative velocity field was absent. Measurements of the flow axial velocity closely upstream of the flame tip revealed that the flame was propagating in a separated or thickened boundary layer [40]. The precise cause for this separation was not clear in their experiment. Nonetheless, Heeger et al. [40] hypothesised that this was due to the development of an adverse pressure gradient along the bluff-body. They attributed this pressure gradient to the decrease of density by combustion and the drop of circumferential velocity component due to the intense mixing with the surrounding air.

It is concluded from this review of the literature that despite some recent advances on understanding flame flashback, this transient phenomenon remains largely unexplored. In an attempt to obtain further understanding of the fundamental physics of flame flashback, this paper considers the behaviour of the static pressure field during flame flashback. Simultaneous pressure measurements on the surface of the bluff-body and high speed flame luminosity imaging are used to characterise the evolution of the static pressure field. Further, the theory of Ishizuka [22] is extended to a case of confined flame with central bluff-body, similar to the configuration investigated experimentally. It is shown that the theory, although highly simplified, can explain the generation of adverse pressure gradient.

Experimental Analysis

Experimental setup

Flame flashback was investigated in an unconfined, swirling, lean, premixed, bluff-body stabilized flame. The burner, Fig. 1, was described in detail in Schneider et al. [41]. Modifications to enable detailed observation of flame flashback were described in Nauert et al. [42]. Therefore only the important features are listed here. Methane and air are mixed inside the plenum prior to entering the radial swirler and the exit nozzle. The movable block design allowed the geometric swirl number to be varied between 0 and 2 by rotating the movable block with a stepper motor. To enable optical access the exit nozzle was made from quartz. For the measurements presented in this paper, the Reynolds number, based on the hydraulic diameter of the nozzle, was 10 000 and the equivalence ratio was set to 0.833. The onset of flashback was induced by increasing the swirl number during operation. This was investigated by Nauert et al. [42] and correlations between the critical swirl number and equivalence ratio as well as that between the critical swirl number and Reynolds number were experimentally determined. Static gauge pressure was measured on the surface of the bluff-body using piezo-resistive pressure transducers (Omega PX409) with a maximum capacity of 2491Pa. To accommodate the pressure transducers and protect them from the hot flow, the bluff-body design was modified. Eight pressure measurement ports with a diameter of 1mm in

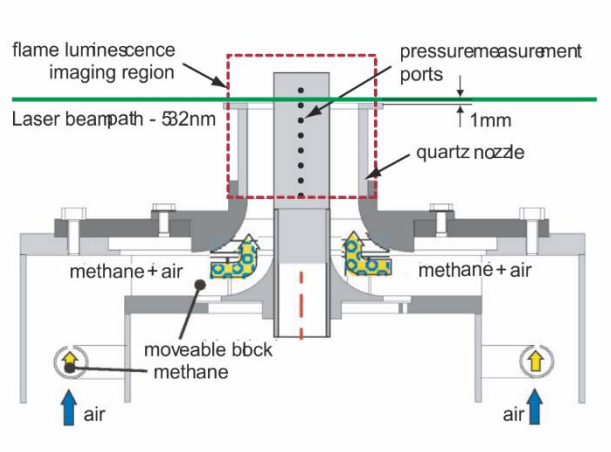

Figure 1: Schematic of the premixed swirl burner

increments of 10mm were installed axially in the water cooled bluff-body, see Fig. 1. These were connected to pressure transducers by copper tubes with equal length of 300mm. In the course of the experimental study,

pressure was measured simultaneously at different ports along the bluff-body (see Fig. 1). However, all the results, presented in this paper are limited to the measurements on the port located 20mm upstream of the top edge of the quartz nozzle. This is because the current study is concerned with the pressure changes across the reactive front in a confined configuration. This required single point pressure measurement inside the quartz nozzle. Further, as the flame penetrates deeply inside the nozzle thermoacoustic instabilities are initiated and mask the pressure changes across the flame. Thus, the few ports close to the upper edge of the quartz nozzle were most suitable for the intended measurements. Other performed investigations (not reported here) aim to understand the correlations between pressure signals recorded at different points along the bluff-body. The total measurement period was 1s and started shortly before flashback. As confirmed by high speed imaging, flame propagation upstream occurs in a small fraction of a second. Hence this period was certainly enough to capture the whole flashback event. The analogue voltage signal was digitised and recorded using an oscilloscope (Tektronix) at 2MHz.

Information about the global flame position and structure were acquired by recording FL with a high speed CMOS camera (HSS5) at 5 kHz frame rate. The imaging region was 60mm × 60mm, covering the entire transparent nozzle. These measurements were taken with simultaneous and time correlated acquisition of the pressure transducer signals. Since FL is a line-of-sight technique, in a separate experiment the pressure measurements were complemented by high speed 1D Rayleigh imaging as a localised flame front detection close to one of the pressure ports [43]. Following a calibration in air, flow and flame temperatures can be deduced directly from the gas densities measured by the Rayleigh scattering method.

Experimental results

Figure 2 shows a pressure history measured 20mm upstream of the nozzle exit. This time trace can be divided into three distinctive time intervals. The first part extends from the beginning of the measurement for about 400ms. Within this time the flame is still downstream of the pressure measurement port. This interval includes very low amplitude oscillations. In keeping with the swirling nature of the flow, the average gauge pressure in this part is slightly negative. As the second interval begins, the fluctuations start to grow and quickly reach large amplitudes. This part is a transition between interval one and three and lasts approximately 100ms. Flame upstream propagation occurs in a fraction of this period. Finally organised pressure oscillations are developed. These are self-sustaining limit-cycles which continue until the flame is extinguished by shutting off the fuel line. This qualitative trend was observed in all flashback realisations.

Spectral analysis of the time trace reveals that the oscillations at the first part happen in a range of frequencies, see Fig. 3. As can be seen in this figure, there is no dominant frequency in this period and the pressure fluctuations are essentially random. The second time interval is very short (almost 100 ms). Using conventional spectral analysis in such a short period results in a poor spectral resolution. Parametric (model based) methods of spectral analysis were therefore used [44]. These methods improve the spectral resolution of the short length data compared to that obtained by standard techniques (non-parametric) [44]. Applying these techniques to the second interval shows that the spectrum of the second interval tends to have more well-defined peaks. Thus the pressure fluctuations happen at more distinctive frequencies compared to the first interval. The main oscillation frequencies are 70, 102 and 146 Hz.

The spectrum of the third part of the pressure trace includes a single frequency at 130 Hz and its harmonic at 260 Hz. This is in complete agreement with the previous measurements of chemiluminescence of the flame after flashback while stabilised inside the burner [42]. Under this condition, the measurements showed that the chemiluminescence oscillates at 130 Hz. Thus the flame after flashback develops thermoacoustic instability and the pressure fluctuations go under limit-cycles. However, through examination of the pressure history and corresponding spectra it is not clear at which stage the thermoacoustic instabilities are initiated. The crucial question here is whether these instabilities lead the upstream flame motion or lag it. In the first case, the thermo-acoustic instability can be a driving mechanism of flashback. However, if thermoacoustic instability follows the flame flashback, it is simply a consequence of the modification of the flow field and has no significant driving impact.

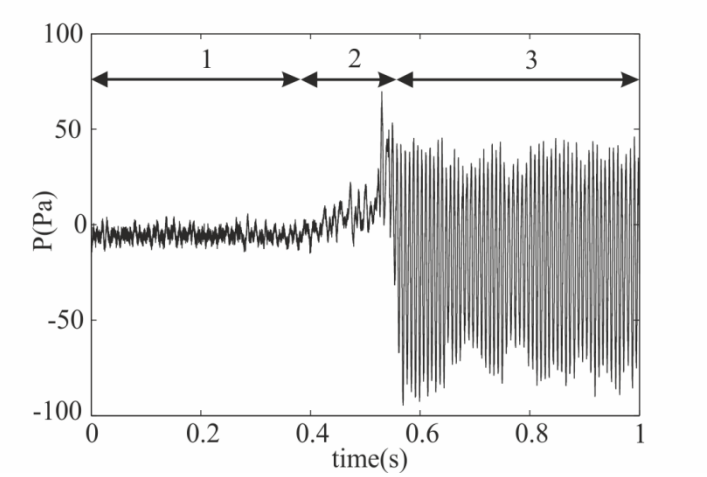

Figure 2: Pressure trace, 1: before flashback, 2: transition period, 3: after flashback.

To precisely clarify the behaviour of the pressure field during flashback, pressure measurement was done simultaneously with high speed FL imaging at 5 kHz. Figure 4 shows a sequence of flame images at various stages of flame flashback. In this measurement the camera system was synchronised with the data acquisition system through an optical trigger. The time axes appearing in the pressure traces show the time relative to this trigger and

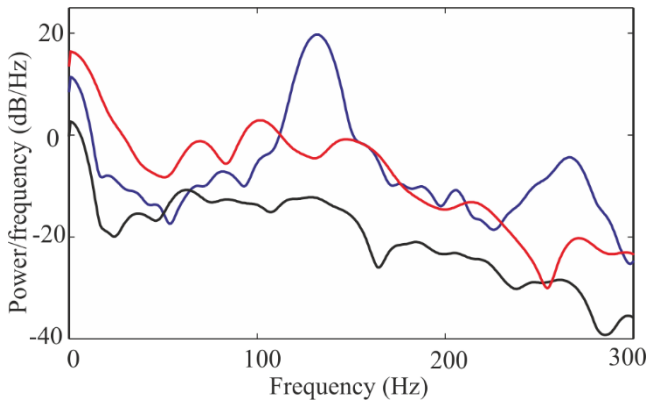

Figure 3: Power spectral density of segments 1-3 in Fig. 2, black: 1, red: 2, blue: 3.

therefore include negative values. It is clear in Fig. 4 that, as expected, when the flame is far downstream of the measurement port, the recorded pressure is negative (Fig. 4a). As the flame upstream propagation continues and reaches close to the measurement point, the pressure starts to rise (Figs. 4b and c). This gain of pressure continues as the flame front passes over the pressure measurement port (Figs. 4d and e). Although not shown in this figure re-exposure of the measurement point to non-reactive flow results in a drop of the gauge pressure. Thus, the simultaneous pressure and FL imaging indicates that the static pressure increases behind the reactive front.

This behaviour of the pressure field is in agreement with the theory of vortex bursting and flame back pressure [17, 22]. Considering the present experimental conditions of bulk axial velocity of 5m/s and swirl number of about 1, Eq. 1 predicts a pressure gain of between 20 and 30Pa. These values are similar to those measured in the present investigation. Interestingly, previous measurements of the pressure behind a flame front propagating in a vortex tube [17], feature qualitative similarities to the present results. In the following sections of this paper, we develop a more advanced theory of vortex bursting which further supports this observation.

Similar images of flame flashback show that such correlation between the pressure and flame propagation continues till the flame reaches the bottom of the nozzle. At this stage the whole length of the nozzle is filled by the reactive flow. Strong pressure pulses are initiated under this condition and very quickly (in less than 50 ms) grow in amplitude. This is then followed by pressure limit-cycles (Fig. 4f). It is, therefore, inferred that thermo-acoustic instability is established only after the flame flashback. Thus, under the investigated conditions the thermoacoustic instability seemed to be a subsequent result of the flashback and is not, by itself, a significant driving mechanism.

The gain of pressure across the flame can have important influences upon the upstream flame propagation. It acts as a support of the front propagation against the incoming flow [22]. In general, this is a known mechanism for enhancement of the flame propagation speed in vortical flows [17]. In the present study the existence of the bluff-body adds further complexities to the problem. The most significant effects are the modification of the vortex and the introduction of a boundary layer. High speed flame imaging clearly shows that the flame propagates close to the surface of the bluff-body. It is, therefore, most probable that the state of the boundary layer greatly affects the flame flashback. As the recent measurements [40] show, flashback in this configuration is associated with either a separated or thickened boundary layer. On the other hand, the present results indicate the development of an adverse pressure gradient on the surface of the bluff-body. This results in the depletion of the momentum flow and may ultimately separate the boundary layer. The flame can then readily propagate in the resultant low velocity region. Nonetheless, in the absence of simultaneously acquired data on the flow velocity, this remains as a possibility.

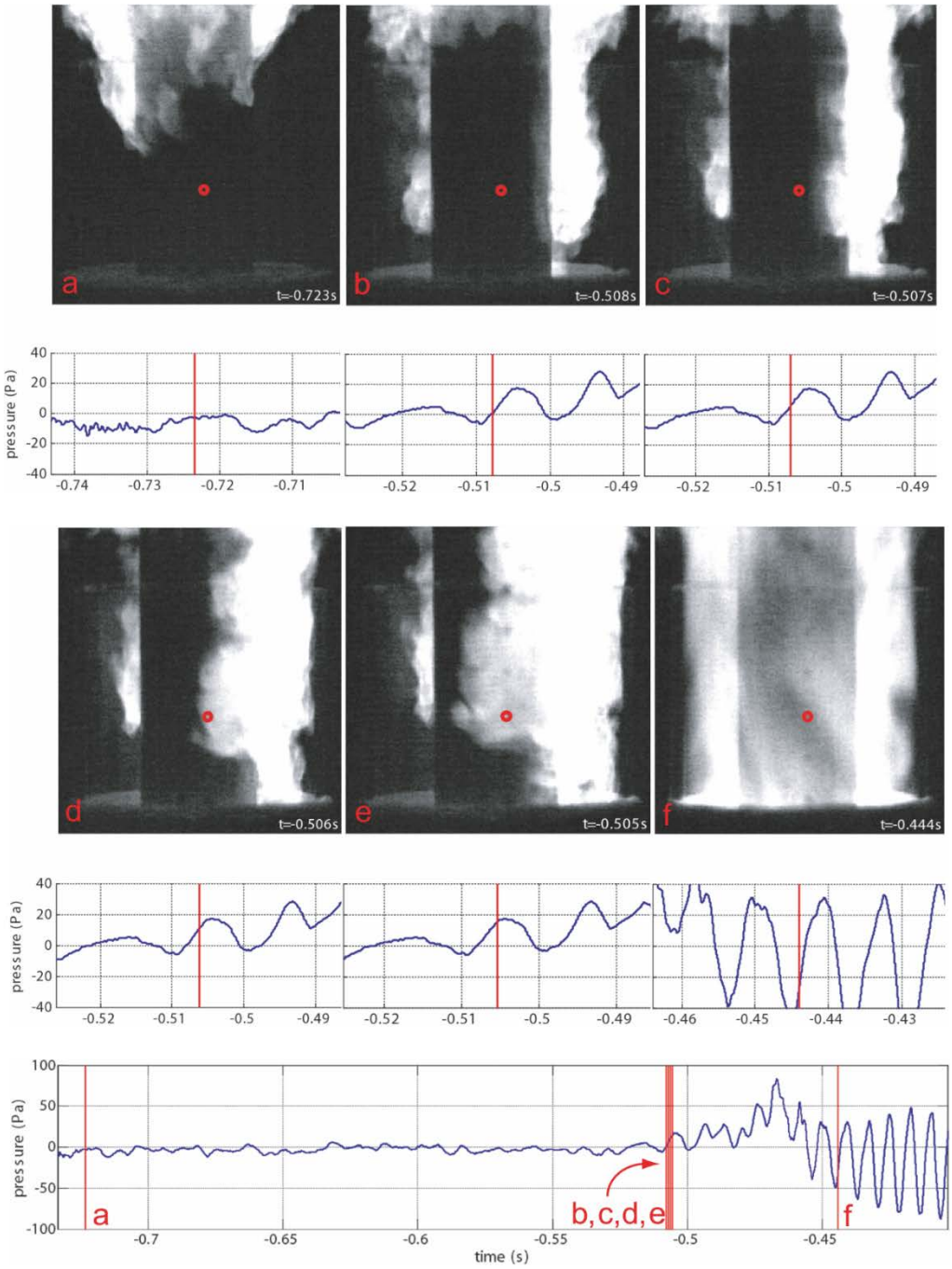

Figure 4: Sequence of flame upstream propagation and the corresponding values of pressure. Red circle: the measurement port. Time axes are relative to the trigger.

Rayleigh scattering was also used to improve the flame detection technique. Although not shown here, consistent with the theoretical expectations, the flame featured a thin flamelet structure. In comparison with FL, Rayleigh imaging provides a more accurate method for detection of the hot flow in front of the pressure measurement ports. However, for quantitative comparison with the pressure signal the Rayleigh measurements should be done inside the transparent nozzle. This is because outside of the nozzle the back pressure effect is significantly interrupted by other pressure fluctuations. These include pressure fluctuations by sudden flow

expansion and also intense mixing with the ambient air. Accurate Rayleigh measurements inside the tube remains as a task for future investigations.

Theoretical analysis

The original theory of vortex bursting was formulated for an unconfined vortex tube [17]. Later, Heeger et al [40] argued that the existence of a surrounding tube and a bluff-body can have a strong influence upon the flow. The argument of Heeger et al [40] was more and less speculative and did not include a rigorous model development. The ensuing analysis aims at addressing this shortcoming. It builds upon that presented by Ishizuka et al. [17] and advances their theory to a confined flame with a central bluff body. This configuration is similar to that investigated, earlier, experimentally. To make analytical progress, Ishizuka et al. [17] and the current extension of their theory consider laminar flows and make a number of simplifying assumptions. Consequently, the theoretical results are not quantitatively comparable with the experiment. Instead, the present theoretical investigation aims at providing further physical understanding of the underlying mechanisms responsible for flame flashback. In particular, it is shown that, in the configuration shown in Fig.1, flame flashback is associated with the development of an adverse pressure gradient across the flame.

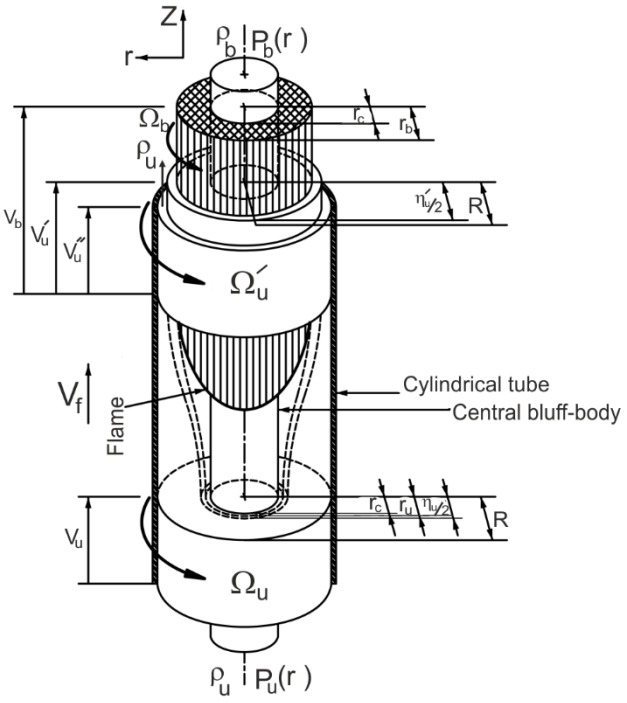

Figure 5: Schematic of the theoretical model

Figure 5 shows the schematic of the flow configuration under investigation. In an attempt to resemble the experimental rig (Fig. 1), the flow configuration in Fig. 5 consists of a rotating flow in a cylinder with a central bluff-body. The swirling flow features a combined axial and vortical motion. The axial velocity is assumed uniform in the radial direction and the tangential velocity is of the Rankine form. Chemical reactions are assumed to be limited to the forced vortex core. The flow is, therefore, divided into three regions: the burned

forced vortex, the unburned forced vortex and the unburned free vortex. Each of these regions is a stream-tube and defines a control volume to which the conservation equations are applied. During flashback the flame moves upstream. Thus, the control volumes of the burned forced vortex, unburned forced vortex and unburned free vortex also move upstream with a velocity equal to the flame velocity $\boldsymbol{V_f}$.

Governing equations and assumptions

The conservation of mass and angular momentum for a non-deformable control volume moving at constant velocity are respectively written as

$$\iint \rho(\boldsymbol{V_r} \cdot \boldsymbol{n}) dA = 0, \qquad (2)$$

$$\iint (\boldsymbol{V} \times \boldsymbol{r}) \rho(\boldsymbol{V_r} \cdot \boldsymbol{n}) dA = 0. \qquad (3)$$

The symbols used in the current analysis are defined in the nomenclature. In Eqs. 2 and 3, $\boldsymbol{V_r}$ is the velocity of the flow relative to a frame of reference attached to the control volume moving at the constant velocity $\boldsymbol{V_f}$. The velocity $\boldsymbol{V}$ is the absolute velocity of the flow relative to the same fixed frame of reference in which the velocity of the control volume is measured. The conservation of linear momentum is given by

$$\iint \boldsymbol{V} \rho(\boldsymbol{V} \cdot \boldsymbol{n}) dA = -\iint P(r) \boldsymbol{n} dA. \qquad (4)$$

The other equations necessary for the analysis of the swirling flow are the radial momentum equation and the perfect gas law, respectively written as

$$\frac{\partial P}{\partial r} = \rho \frac{{V_\theta}^2}{r}, \qquad (5)$$

$$P = \rho R T. \qquad (6)$$

Throughout this analysis, the axial, radial and tangential velocities are expressed by the following equations

$$V_z = constant\ for\ (0 \leq \mathrm{r} \leq \mathrm{R}), \qquad V_r = 0, \qquad (7)$$

$$V_\theta = \begin{cases} \Omega r\ for\ \left(0 \leq \mathrm{r} \leq \frac{\eta_u}{2}\right) \\ \frac{\Omega {\eta_u}^2}{4r}\ for\ \left(\frac{\eta_u}{2} \leq \mathrm{r} \leq R\right) \end{cases}. \qquad (8)$$

Equation 8 expresses the circumferential velocity generated by the well-known Rankin vortex. Further, the following semi-empirical expression is used to define the swirl number [45]

$$SN = \frac{G/2}{1 - G/2}, \qquad (9)$$

in which, $G = \frac{V_{\theta max}}{V_{z max}}$ is the ratio of the maximum tangential velocity to the maximum axial velocity. The axial velocity of the flow far upstream of the flame is taken as $V_{z_{max}} = V_u = YS_u$, which is the axial velocity of the flow just ahead of the flame when the flame is at rest. This is due to the fact that the axial velocity of the flow far upstream of the flame is, in fact, unsteady when the flame is moving upstream [17]. In short, the following assumptions are made throughout this analysis:

- Flow is axisymmetric, laminar, incompressible and inviscid,
- axial flow velocity is uniform in radial direction, the tangential velocity is of Rankine form and the radial velocity is zero,
- flame is laminar and premixed,
- flame speed is constant,
- momentum is conserved during combustion,
- burning is limited to forced vortex region of the flow.

Model development

Equation 2 is, first, applied to the control volumes defined in Fig. 5. This, results in

$$\rho_u(V_u - V_f)\pi(r_u^2 - r_c^2) = \rho_b(V_b - V_f)\pi(r_b^2 - r_c^2) = \rho_u S_u A_f, \qquad (10)$$

for the burned forced vortex, where $\rho_u S_u A_f$ is the mass flux through the flame. Further, conservation of mass in the unburned forced vortex and unburned free vortex, respectively, leads to

$$\rho_u(V_u - V_f)\pi[\left(\frac{\eta_u}{2}\right)^2 - r_u^2] = \rho_u(V_u' - V_f)\pi[\left(\frac{\eta_u'}{2}\right)^2 - r_b^2], \qquad (11) \text{ and,}$$

$$\rho_u(V_u - V_f)\pi\left[R^2 - \left(\frac{\eta_u}{2}\right)^2\right] = \rho_u(V_u'' - V_f)\pi\left[R^2 - \left(\frac{\eta_u'}{2}\right)^2\right]. \qquad (12)$$

Similarly, through application of the angular momentum equation (Eq. 3) the following expressions are developed. These correspond to the burned forced vortex, unburned forced vortex and unburned free vortex regions, respectively.

$$\Omega_u\rho_u(V_u - V_f)(r_u^4 - r_c^4) = \Omega_b\rho_b(V_b - V_f)(r_b^4 - r_c^4), \qquad (13)$$

$$\Omega_u(V_u - V_f)\left[\left(\frac{\eta_u}{2}\right)^4 - r_u^4\right] = \Omega_u'(V_u' - V_f)\left[\left(\frac{\eta_u'}{2}\right)^4 - r_b^4\right], \qquad (14)$$

$$\Omega_u\eta_u^2(V_u - V_f)\left[R^2 - \left(\frac{\eta_u}{2}\right)^2\right] = \Omega_u'\eta_u'^2(V_u'' - V_f)\left[R^2 - \left(\frac{\eta_u'}{2}\right)^2\right]. \qquad (15)$$

Equation 4 is, subsequently, applied to an infinitesimally narrow ring control volume at the wall of the bluff-body and to an infinitesimally narrow ring control volume at the wall of the cylindrical tube. These, result in

$$\rho_b V_b^2 - \rho_u V_u^2 = (\Delta P)_{r=r_c}, \qquad (16)$$

at the bluff-body wall and,

$$\rho_u V_u''^2 - \rho_u V_u^2 = (\Delta P)_{r=R} \qquad (17)$$

at the wall of the cylindrical tube.

Integrating the radial momentum relation (Eq. 5) upstream and downstream of the flame and subtracting the resultant equations yields,

$$(\Delta P)_R - (\Delta P)_{r_c} = \rho_u V_{\theta max}^2\left[1 - \frac{1}{\varepsilon_r^2} + \frac{k'}{2}\left(1 - \frac{\rho_b}{\rho_u}\frac{\varepsilon_r''}{\varepsilon_r'^2}\right) - \frac{k^2}{2}\left(1 - \frac{1}{\varepsilon_r^2}\right)\right]. \qquad (18)$$

In Eq. 18,

$$k' = \mathrm{k}^2 - K'^2,\ \varepsilon_r' = \frac{(\varepsilon_r k)^2 + K'^2}{k^2 + K'^2},\ \varepsilon_r'' = \frac{(\varepsilon_r k)^2 - K'^2}{k^2 - K'^2},\ K' = \frac{r_c}{\frac{\eta_u}{2}}. \qquad (19\ a, b, c, d)$$

and the parameters k, ε_r and $V_{\theta max}$ are, respectively, the burning ratio, the expansion ratio and the maximum tangential velocity in the Rankine combined vortex (see the nomenclature). Substituting Eq. 9 into Eq. 18 renders

$$(\Delta P)_R - (\Delta P)_{r_c} = \rho_u \left(\frac{2\,SN\,V_z}{1+SN}\right)^2 \left[1 - \frac{1}{\varepsilon_r^2} + \frac{k'}{2}\left(1 - \frac{\rho_b}{\rho_u}\frac{\varepsilon_r''}{\varepsilon_r'^2}\right) - \frac{k^2}{2}\left(1 - \frac{1}{\varepsilon_r^2}\right)\right]. \qquad (20)$$

Further, by considering Eq. 10 it can be readily shown that

$$V_u = \mathrm{Y'S_u} + V_f, \qquad (21)$$

$$V_b = \frac{\rho_\mathrm{u}}{\rho_b}\frac{\mathrm{Y'S_u}}{\varepsilon_r^2} + V_f, \qquad (22)$$

where

$$\mathrm{Y'} = \frac{\mathrm{k}^2}{\left(\mathrm{k}^2 - \mathrm{K'}^2\right)} Y\ .$$

Now, substitution of Eq. 21 into Eq. 12 yields

$$\mathrm{V_u''} = \frac{(1-\mathrm{K}^2)\mathrm{Y'S_u}}{1-(\varepsilon_r K)^2} + V_f, \qquad (23)$$

in which $K = \frac{\eta_u/_2}{R}$ is the ratio of the radius of the forced vortex core upstream of the flame to the radius of the cylindrical tube.

A useful parameter in the case of a flow in a cylindrical tube with a central bluff-body is the annulus ratio $AR = \frac{r_c}{R}$ which is defined as the ratio of the radius of the bluff-body to the radius of the cylindrical tube. In the current study the annulus ratio is not used as a parameter in the equations but it can be obtained by the following function which is in terms of the parameters K and K'

$$AR = KK'. \qquad (24)$$

Through substitution of Eqs. 21 and 22 into Eq. 16, the following relation is derived

$$\left[\rho_u\left(\frac{\rho_b}{\rho_u} - 1\right)\right]V_f^2 + \left[2\rho_u Y' S_u\left(\frac{1}{\varepsilon_r''} - 1\right)\right]V_f + \left[\rho_u (Y'S_u)^2\left(\frac{\rho_u}{\rho_b}\frac{1}{\varepsilon_r''^2} - 1\right) - (\Delta P)_{r=r_c}\right] = 0. \qquad (25),$$

Further, substituting Eqs. 21 and 23 into Eq. 17 results in,

$$\left\{2\rho_u Y' S_u\left[\frac{1-\mathrm{K}^2}{1-(\varepsilon_r K)^2} - 1\right]\right\}V_f + \left\{\rho_u (Y'S_u)^2\left\{\left[\frac{1-\mathrm{K}^2}{1-(\varepsilon_r K)^2}\right]^2 - 1\right\} - (\Delta P)_{r=R}\right\} = 0. \qquad (26)$$

Equations 20, 25 and 26 constitute a system of three simultaneous equations and three unknowns. These are the pressure difference across the flame at the wall of the bluff-body $(\Delta P)_{r=r_c}$, the pressure difference across the flame at the wall of the cylindrical tube $(\Delta P)_{r=R}$ and the flame speed V_f. Simultaneous solution of this system of equations reveals

$$(\Delta P)_{r=r_c} = \frac{-b' + \sqrt{b'^2 - 4a'c'}}{2a'}, \qquad (27)$$

$$(\Delta P)_R = \frac{-b' + \sqrt{b'^2 - 4a'c'}}{2a'} + \rho_u \left(\frac{2\,SN\,V_z}{1+SN}\right)^2 \left[1 - \frac{1}{\varepsilon_r^2} + \frac{k'}{2}\left(1 - \frac{\rho_b}{\rho_u}\frac{\varepsilon_r''}{\varepsilon_r'^2}\right) - \frac{k^2}{2}\left(1 - \frac{1}{\varepsilon_r^2}\right)\right], \qquad (28)$$

$$V_f = \frac{(\Delta P)_{r=r_c} + A' - B'}{C'}, \qquad (29)$$

where

$$A' = \rho_u \left(\frac{2\,SN\,V_z}{1+SN}\right)^2 \left[1 - \frac{1}{\varepsilon_r^2} + \frac{k'}{2}\left(1 - \frac{\rho_b}{\rho_u}\frac{\varepsilon_r''}{\varepsilon_r'^2}\right) - \frac{k^2}{2}\left(1 - \frac{1}{\varepsilon_r^2}\right)\right] \qquad (30a)$$

$$B' = \rho_u (Y' S_u)^2 \left\{\left[\frac{1-\mathrm{K}^2}{1-(\varepsilon_r K)^2}\right]^2 - 1\right\} \qquad (30b)$$

$$C' = 2\rho_u Y' S_u \left[\frac{1-\mathrm{K}^2}{1-(\varepsilon_r K)^2} - 1\right] \qquad (30c)$$

$$a' = \rho_u \left(\frac{\rho_b}{\rho_u} - 1\right) \qquad (30d)$$

$$b' = 2\rho_u \left(\frac{\rho_b}{\rho_u} - 1\right)(A' - B') + 2C'\rho_u Y' S_u \left(\frac{1}{\varepsilon_r''} - 1\right) - C'^2 \qquad (30e)$$

$$c' = \rho_u \left(\frac{\rho_b}{\rho_u} - 1\right)(A' - B')^2 + 2C'\rho_u Y' S_u \left(\frac{1}{\varepsilon_r''} - 1\right)(A' - B') + C'^2 \rho_u (Y' S_u)^2 \left(\frac{\rho_u}{\rho_b}\frac{1}{\varepsilon_r''^2} - 1\right) \qquad (30f)$$

The pressure difference across the flame over the cross-sectional area of the cylindrical tube $(\Delta P)_{total}$ is obtained by subtracting the pressure acting on the cross-sectional area of the flow downstream of the flame, P_b, from that acting on the cross-sectional area of the flow upstream of the flame, P_u. The pressures P_u and P_b acting on the cross-sectional areas of the flow are calculated by integrating the pressure over the cross-sectional area of the tube upstream and downstream of the flame respectively. After some algebra, the total pressure difference across the flame can be expressed as,

$$(\Delta P)_{total} = \rho_u {V_{\theta max}}^2 \frac{{K'}^2}{1-{K'}^4}\left\{\frac{{K'}^4}{4}\left(1 - \frac{\rho_b}{\rho_u}\frac{1}{{\varepsilon_r}^4}\right) + \left[\frac{k^2}{2(\varepsilon_r K)^2} - \frac{k^4}{4}\right]\left(1 - \frac{\rho_b}{\rho_u}\right) - \frac{1}{4(\varepsilon_r K)^2}\left(1 - \frac{\rho_b}{\rho_u}\frac{{K'}^2}{2{\varepsilon_r}^2}\right) - \ln(\varepsilon_r)\right\} + (\Delta P)_{r=r_c}. \qquad (31)$$

Finally, substitution from Eq. 9 into Eq. 31 results in

$$(\Delta P)_{total} = \rho_u \left(\frac{2\,SN\,V_{z_{max}}}{1+SN}\right)^2 \frac{{K'}^2}{1-{K'}^4}\left\{\frac{{K'}^4}{4}\left(1 - \frac{\rho_b}{\rho_u}\frac{1}{{\varepsilon_r}^4}\right) + \left[\frac{k^2}{2(\varepsilon_r K)^2} - \frac{k^4}{4}\right]\left(1 - \frac{\rho_b}{\rho_u}\right) - \frac{1}{4(\varepsilon_r K)^2}\left(1 - \frac{\rho_b}{\rho_u}\frac{{K'}^2}{2{\varepsilon_r}^2}\right) - \ln(\varepsilon_r)\right\} + (\Delta P)_{r=r_c}, \qquad (32)$$

where $V_{z_{max}} = Y S_u$.

The validity of these solutions is verified in Appendix A. It is demonstrated that in the asymptotic limit of very large confining cylinder and a very thin bluff-body the current analytical results reduce to those presented by Ishizuka [22].

Discussion

Table 1 summarises some of the numerical values of the parameters used in the analysis of the solutions developed in the previous section.

Table 1: Values of the parameters used in the theoretical analysis

$\frac{\rho_u}{\rho_b}$	$\mathrm{K} = \frac{\eta_u/2}{\mathrm{R}}$	Y	k	SN	$\mathrm{K}' = \frac{\mathrm{r_c}}{\eta_u/2}$
7	0.2 (as SN or K' vary)	4	0.8	1 (as K or K'vary)	0.5 (as SN varies)

The pressure difference across the flame is non-dimensionalised with respect to the pressure of the unburned gas far upstream of the flame $P_u = 10^5\ Pa, (i.e. \overline{\Delta P} = \left(\frac{1}{P_u}\right)\Delta P = \left(\frac{1}{P_u}\right)(P_u - P_b))$. The flame speed is scaled with respect to the laminar burning velocity $S_{u\,(CH_4)} = 0.4$ m/s of a stoichiometric air-methane mixture burning at the pressure of 1atm [45]. That is $\overline{V_f} = \frac{V_f}{S_{u\,(CH_4)}}$. Further, the laminar burning velocity is non-dimensionalised with respect to the density of air, $\rho_u = 1.225$ kg/m^3 and pressure $P_u = 10^5$ Pa of the unburned gas far upstream of the flame. This is $\overline{S_u} = \left(\frac{\rho_u}{P_u}\right){S_u}^2$. For common hydrocarbon mixtures such as air-methane and air-propane mixtures the laminar burning velocity is $S_u \cong 0.4ms^{-1}$ which corresponds to a non-dimensional burning velocity of $\overline{S_u} \cong 2 \times 10^{-6}$.

Figure 6 shows the effect of swirl number on the pressure difference across the flame for a range of reactive mixtures. Flow configurations with bluff-body (Figure 6a) and without bluff-body (Figure 6b) are considered. In Figure 6a the pressure is calculated on the surface of the bluff-body while in Figure 6b this is calculated on the centreline. These figures show that under both flow configurations and all reactive mixtures a noticeable adverse pressure gradient develops across the flame.

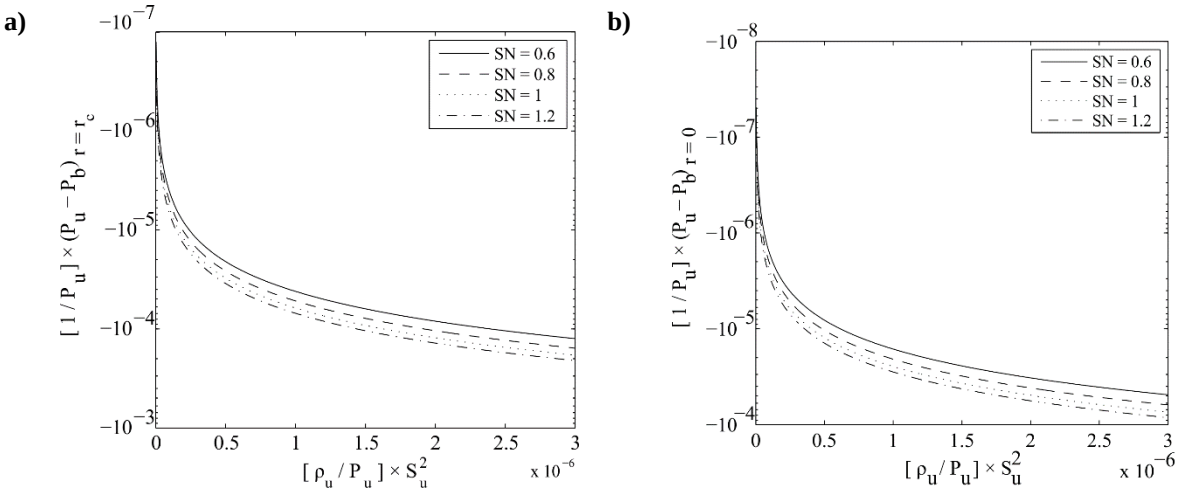

Figure 6: Effect of the swirl number on the pressure difference across the flame for various mixtures a) on the surface of the bluff-body for the configuration with bluff-body and b) on the burner centreline for the configuration without bluff body.

As expected, in both cases shown in Fig.6, for a non-reactive mixture (i.e. $\overline{S_u} = 0$) the pressure differences reduce to zero. The absolute value of these differences quickly increases with an increase in the laminar flame

speed. Further, the adverse pressure gradient increases with an increase in the swirl number. Once again, this is to be expected as higher swirl numbers feature stronger centrifugal forces and therefore more pronounced pressure differences between the burned and unburned regions. A comparison between figures 6a and 6b, further, reveals that the presence of a bluff-body intensifies the pressure difference across the flame. For a typical hydrocarbon mixture with $\overline{S_u} \cong 2 \times 10^{-6}$, Fig.6a indicates that the pressure difference on the surface of the bluff-body is of order 10 Pa. This value is within the same order of magnitude as the measurements reported in Fig. 4.

Figure 7 shows the influence of swirl number and laminar flame speed upon the flame propagation speed in both configurations, with and without the bluff-body. Similar to that observed in Fig. 6, swirl number has an intensifying effect and an increase in the propagation speed of the flame is observed at higher swirl numbers. Figures 7a and 7b clearly show that the propagation speed appears to be strongly dependent upon the laminar flame speed. Further, the configuration with the bluff-body (Fig. 7a) features a considerably higher propagation speed compared to that without the bluff-body (see Fig 7b).

Figures 8a and 8b respectively show the effect of the ratio of the bluff-body radius and the radius of the cold vortex core, upon the pressure difference across the flame and the flame speed. In keeping with the results shown in Figs. 6 and 7, Fig. 8 shows that introducing a bluff-body increases the pressure difference across the flame and the flame propagation speed. In addition to this, the ratio of the bluff-body radius and cold vortex core has a significant impact on the developed adverse pressure gradient and flame propagation speed. This can be briefly explained as follows. Holding the parameters in Table 1, constant does not allow the flame area A_f and the radius of the unburned mixture that passes through the flame r_u to change as the radius of the bluff-body varies. Thus, the mass flux through the flame is constant for a given mixture as the radius of the bluff-body changes. Conservation of mass (Eq. 10), then, requires that the flame speed increases as the radius of the bluff-body increases from zero (no bluff-body) to a finite value.

Overall, the presented theoretical analysis shows the significant role of confinement and inclusion of the bluff-body on the extent of the adverse pressure gradient across the flame and flame propagation velocity. Further, the predicted numerical values are within the same order of magnitude as those measured experimentally. The theoretical analysis is rather simple and includes a number of assumptions. In particular, it assumes an axisymmetric, laminar flow and flame. Nonetheless, these assumptions are apparently violated in the experiment. Importantly, the bulk flow in the experiment is turbulent. Thus, the similarity of the numerical outcomes of the model with their experimental counterparts sounds surprising. To explain this, it could be postulated that the reactive flow in the boundary layer is mostly laminar and, therefore, consistent with the theoretical assumptions. Verification of this hypothesis, of course, requires further experimental investigations on the state of the flow and flame in the proximity of the wall. Even regardless of this, the model is useful in developing a more rigorous understanding of the underlying physics of flame flashback. The authors are currently concerned with the conduction of more sophisticated theoretical analyses and further measurements, to better understand this phenomenon.

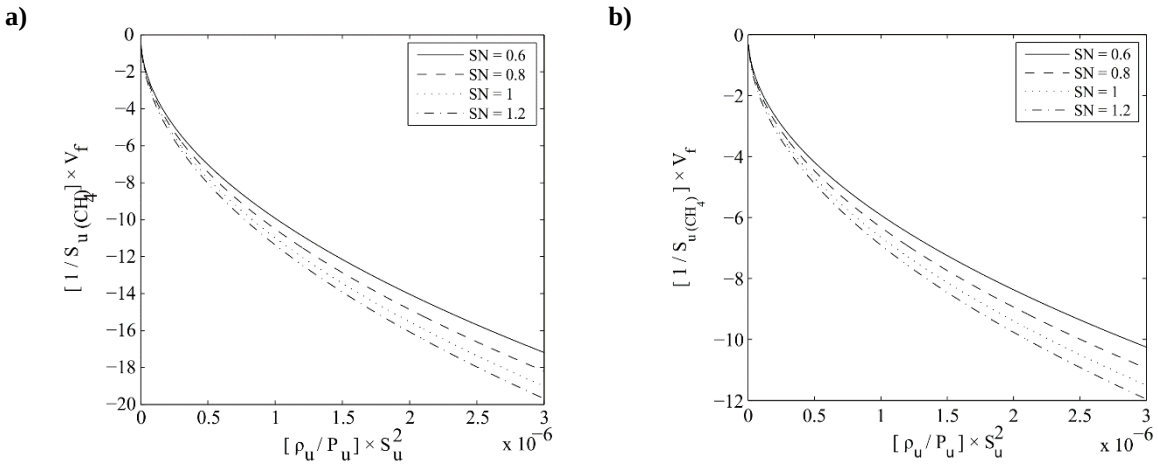

Figure 7: Effect of the swirl number on the flame speed for various mixtures a) with bluff-body, b) without bluff-body.

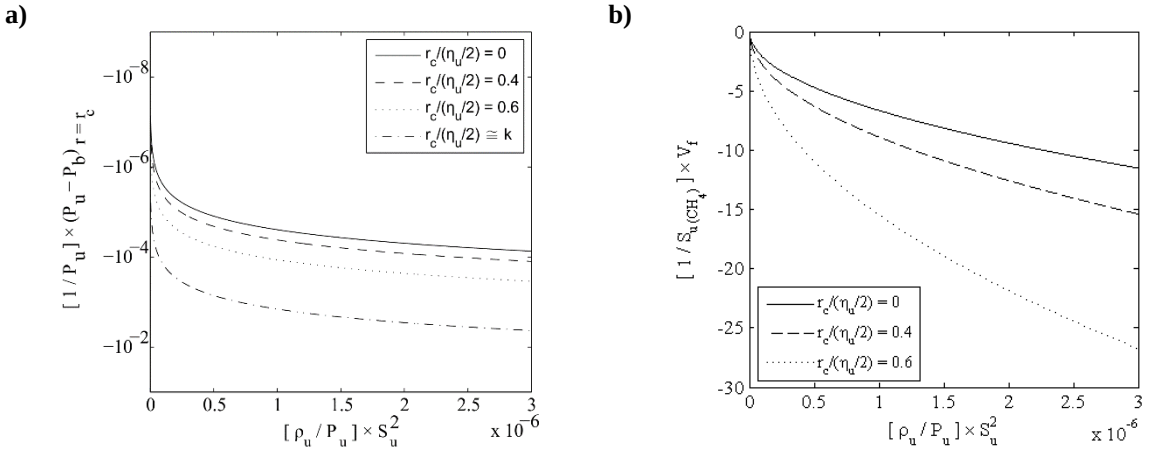

Figure 8: Effect of the ratio of the radius of the bluff-body and the cold vortex core on a) the pressure difference across the flame on the surface of the bluff-body and b) the flame speed, for various mixtures.

Conclusions

Flashback of premixed swirling flames was investigated experimentally and theoretically. The objective was to elucidate the physical mechanisms responsible for the upstream flame propagation. Static gauge pressure on the surface of the bluff-body was measured as flame flashed back. This was accompanied, simultaneously, by high speed flame luminosity imaging. Pressure traces showed that in the course of measurement, oscillations in pressure grow and lead to large amplitude fluctuations. These had a dominant frequency which matched very well the previously measured flame chemiluminescence under the same experimental conditions. Close inspection of the flame images during upstream propagation revealed that the static pressure increases behind the flame front. This was in keeping with the general theory of vortex bursting [22]. In order to make this theory more comparable to the experiment, the original theory was extended to include confinement and central bluff-body. It was observed that inclusion of these had a pronounced intensifying effect on the strength of the adverse pressure gradient. The developed model was relatively simple and restricted to a number of assumptions. Yet,

the theoretical values of the pressure difference across the flame, are within the same order of magnitude as those measured experimentally. These similarities motivate further experimental and theoretical investigations on this problem.

Acknowledgements

The authors are very grateful for financial support by Deutsche Forschungsgemeinschaft through project KA 3483/1-1. Andreas Dreizler is grateful for generous support through the Leibniz-program of Deutsche Forschungsgemeinschaft.

Nomenclature

AR	Annulus ratio$\equiv \frac{r_c}{R}$
A_f	Surface area of flame
k	Burning ratio$\equiv \frac{r_c}{\eta_{u/2}}$
K	$\equiv \frac{\eta_u/2}{R}$
n	Normal unit vector
r	Radial coordinate
r_u	Radius of unburned mixture upstream of the flame which will burn in the flame
r_b	Radius of burned mixture downstream of the flame
r_c	Radius of central bluff-body
R	Radius of cylindrical tube
$P(r)_u$	Pressure on axis at radial distance r from swirl axis upstream of the flame
$P(r)_b$	Pressure on axis at radial distance r from the swirl axis downstream of the flame
P_u	Pressure on cross-sectional area upstream of the flame
P_b	Pressure on cross-sectional area downstream of the flame
$(\Delta P)_{r=0}$	Pressure difference across the flame at the vortex axis
$(\Delta P)_{r=R}$	Pressure difference across the flame at the wall of the cylindrical tube
$(\Delta P)_{r=r_c}$	Pressure difference across the flame at the wall of the central bluff-body
$(\Delta P)_{total}$	Pressure difference across the flame over the total cross-sectional area of the flow
$\overline{\Delta P}$	Non-dimensional pressure difference across the flame
S_u	Laminar burning velocity
$\overline{S_u}$	Non-dimensional laminar burning velocity

$\mathbf{V}$	Velocity vector
V_f	Flame speed
$\bar{V_f}$	Non-dimensional flame speed
V_z	Axial velocity
V_θ	Tangential velocity
V_r	Relative velocity
V_u	Axial velocity of unburned mixture upstream of the flame
V_b	Axial velocity of burned mixture downstream of the flame in forced vortex core
$V_u{}'$	Axial velocity of unburned mixture downstream of the flame in forced vortex core
$V_u{}''$	Axial velocity of unburned mixture downstream of the flame in free vortex core
Y	Ratio of the flame area A to the cross sectional area of the unburned mixture$\equiv \frac{A_f}{(\pi r_u^2)}$
Ω	Angular velocity
Ω_u	Angular velocity of unburned mixture upstream of the flame
Ω_b	Angular velocity of burned mixture downstream of the flame
$\Omega_u{}'$	Angular velocity of unburned mixture downstream of the flame
η	Diameter of forced vortex core
η_u	Diameter of forced vortex core upstream of the flame
$\eta_u{}'$	Diameter of forced vortex core downstream of the flame
SN	Swirl number
ε_r	Expansion ratio$\equiv \frac{r_b}{r_u}$
ρ_u	Density of unburned gas
ρ_b	Density of burned gas

References

1- Mongia, H.C., Held, T.J., Hsia, G. C., Panadali, R. P., Challenges and progress in controlling dynamics in gas turbines, J. Propulsion Power, 19(2003): 822-829.

2- Karimi, N., Response of a conical, laminar premixed flame to low amplitude acoustic forcing- A comparison between experiment and kinematic theories, Energy (2014), doi:10.1016/j.energy.2014.10.036.

3- Lieuwen T., J., Modeling premixed combustion-acoustic wave interaction: A review, Propulsion Power, 19(2003):765-781.

4- Sommerer Y., Galley D., Poinsot T., Ducruix S., Lacas F., Veynante D., Large eddy simulation and experimental study of flashback and blow-off in lean partially premixed swirled burner, J. Turbulence 5(2004):1-21.

5- Lewis, B., von Elbe, G., *Combustion, Flames and Explosion of Gases*, Academic Press, New York, 1951.

6- Plee, S. L., Mellor, A. M., Review of flashback reported in pre-vaporizing/Premixing combustors, Combut. Flame, 32(1978):193-203.

7- Coats, C.M., Combust. Flame, Comments on "Review of flashback reported in pre-vaporizing/premixing combustion" 37(1980): 331-333.

8- Fritz J., Kröner, M., Sattelmayer T., Flashback in a swirl burner with cylindrical premixing zone, J. Eng. Gas Turbine Power, 126(2004): 276-283.

9- Kröner, M., Fritz J., Sattelmayer T., Flashback limits for combustion induced vortex breakdown in a swirl burner, J. Eng. Gas Turbine Power, 125(2003):693-700.

10- Konle M., Kiesewetter F., Sattelmayer T., Simultaneous high repetition rate PIV-LIF measurement of CIVB driven flashback, Exp. Fluids 44(4)(2008): 529-538.

11- Kiesewetter F., Konle M., Sattelmayer T., Analysis of combustion induced vortex breakdown driven flame flashback in a premix burner with cylindrical mixing zone, J. Eng. Gas Turbine Power, 129(2007): 929-936.

12- Poinsot, T., Veynante, D., *Theoretical and Numerical Combustion*, Second Edition, Edwarsd, Inc. Philadelphia, PA, 2005.

13- Cantwell, B., Organized motion in turbulent flow, Ann. Rev. Fluid Mech. 13(1981): 457-515).

14- Gruber A., Sankaran, R., Hawkes E. R., Chen J. H., Turbulent flame-wall interaction: a direct numerical simulation, J. Fluid. Mech., 658(2010): 5-32.

15- Chomiak J., Dissipation fluctuations and the structure and propagation of turbulent flames in premixed gases at high Reynolds numbers, Proc. Combust. Inst. 16(1977):1665-73.

16- McCormak P. D., Scheller K., Mueller G., Tisher R., Flame propagation in a vortex core, Combust. Flame 19(2) (1972):297-303.

17- Ishizuka S., Flame propagation along a vortex axis, Prog. Energy Combust. Sci. 28(2002): 477-542.

18- Daneshyar HD., Hill PG., The structure of small-scale turbulence and its effect on combustion in spark ignition engines. Prog. Energy Combust. Sci., 65(1987): 291-312.

19- Asato K., Himura T., Wada H., Takeuchi Y., Characteristics of flame propagation in vortex core: validity of model or flame propagation. Combust. Flame 110(1997):418-428.

20- Atobiloye RZ., Britter RE, on flame propagation along vortex tube. Combust. Flame, 98(1994): 220-230.

21- Sakai Y., Ishizuka S., The phenomena of flame propagation in a rotating tube, 26(1996): 847-853.

22- Ishizuka S., Hamasaki T., Koumura K., Hasegawa R., Measurements of flame speeds in combustible vortex rings: validity of the back-pressure drive flame propagation mechanism. Proc Combust Inst. 27(1998): 727-734.

23- Ishizuka S., Koumura K., Hasegawa R., Enhancement of flame speed in vortex rings of rich hydrogen/air mixtures in air., Proc. Combust. Inst., 28(2000):1949-1956.

24- Ashurst WmT., Flame propagation along a vortex: the baroclinic push. Combust Sci., Technol., 112(1996): 175-185.

25- Umemura A., Takamori S., Wave nature in vortex bursting initiation. Proc Combust. Inst., 28(2000): 1941-1948.

26- Umemura A., Takamori S., Rapid flame propagation in a vortex tube in perspective of vortex breakdown phenomena. Combust Flame 125(2001): 820-838.
27- Hasegawa T., Nakamichi R., Nishiki S., Mechanism of lame evolution along a fine vortex. Combust. Theory Modelling, 6(2002): 413-424.
28- Keller, J.O., Vaneveld L., Kroschelt, D., Hubbard, G. L., Ghoniem, A. F., Daily, J. W., Oppenheim A. K., AIAA J.20(1981): 254-262.
29- Thibaut D., Candel S., Numerical study of unsteady turbulent premixed combustion: application to flashback simulation, Combust. Flame 113(1998): 53-65.
30- Candel, S., Combustion dynamics and control: progress and challenges. Proc Combust. Inst., 29(2002): 1-28.
31- Poinsot TJ., Trouve A.C., Veynante D.P., Candel S., Esposito E.J., Vortex driven acoustically coupled combustion instabilities., J. Fluid Mech. 177(1987): 265-292.
32- Candel S., Durox D., Ducruix S., Birbaud, A.L., Noiray, N., Schuller, T., Flame dynamics and combustion noise: progress and challenges., Int. J. Aeroacoustics, 8(1)(2009): 1-56.
33- Karimi, N., Brear, M. J., Jin, S. H., Monty, J. P., Linear and non-linear forced response of a conical, ducted, laminar premixed flame. Combustion and flame, 156(11) (2009), 2201-2212.
34- Karimi, N., Brear, M. J., Moase, W. H., On the interaction of sound with steady heat communicating flows. Journal of Sound and Vibration, 329(22) (2010), 4705-4718.
35- Lucca-Negro O, O' Doherty T., Vortex breakdown: a review, Prog. Energy Combust. Sci., 27(2000):431-48.
36- Escudier M., Vortex breakdown: observations and explanations. Prog. Aerospace Sci., 25(1988): 189-229.
37- Leibovich S., The structure of vortex breakdown, Ann. Review Fluid Mech., 10(1978): 221-246.
38- Kröner M., Sattelmayer T., Fritz J., Kiesewetter F., Hirsch C., Flame propagation in swirling flows-effect of local extinction on combustion induced vortex breakdown., Combust. Sci. and Tech. 179(2007): 1385-1416.
39- Konle M., Sattelmayer T., Time scale model for the prediction of the onset of flame flashback driven by combustion induced vortex breakdown (CIVB), Proc. ASME Turbo. Expo. GT 2009-59606 (2009).
40- Heeger C., Gordon R. L., Tummers M. J., Sattelmayer T., Dreizler A., Experimental analysis of flashback in lean premixed swirling flames: upstream flame propagation. Exp. Fluid., 49(2010):853-863.
41-Schneider C., Dreizler A., Janika J., Fluid dynamical analysis of atmospheric reacting and isothermal swirling flows, 74(1)(2005): 103-127.
42- Nauert, N., Petersson P., Linne, M., Dreizler,A., Experimental analysis of flashback in lean premixed swirling flames: conditions close to flashback., Exp. Fluids, 43(2007): 89-100.
43- Bork, B., Böhm, B., Heeger, C., Chakravarthy, S.R., Dreizler, A., 1D high-speed Rayleigh measurements in turbulent flames; Appl. Phys. B 101(2010), 487 – 491.
44- Kay, S., Marple, S. L., Spectrum analysis-A modern perspective, Proc. IEEE, 69(11)(1981): 1380-1420
45- Gupta AK, Lilley DG, Syred N. Swirl Flows. Kent: Abacus Press; 1984.

Appendix A: Validity of the theoretical model

Equations 27, 28 and 29 contain the new parameters K and K' compared to the equivalent relations derived by Ishizuka et al [17]. The parameter K' is defined as the ratio of the radius of the bluff-body r_c to the radius of the

forced vortex core upstream of the flame $\frac{\eta_u}{2}$. The model of Ishizuka et al [17] can be considered as a swirling flow in a cylindrical tube of infinitely large radius, $i.e\ R \to \infty$, and with a bluff-body of infinitely small radius ($r_c \to 0$). Thus, it is expected that by setting $R \to \infty$ ($K = 0$) and $r_c \to 0$ ($K' = 0$) in Eqs. 19a-d and 30a-f, the Eqs. 27, 28 and 29 simplify to those derived by Ishizuka et al [17].

Setting $K = 0$ and $K' = 0$ in Eqs. 19a-d and 30a-f reveals

$$\varepsilon_r' = \varepsilon_r'' = \varepsilon_r^2, \qquad \text{(A-1)}$$

$$k' = k^2,$$

$$A' = \rho_u \left(\frac{2\,SN\,V_z}{1+SN}\right)^2 \left[1 - \frac{1}{\varepsilon_r^2} + \frac{1}{2}\left(1 - \frac{\rho_b}{\rho_u}\right)\frac{k^2}{\varepsilon_r^2}\right], \qquad \text{(A-2)}$$

$$B' = 0, \qquad \text{(A-3)}$$

$$C' = 0, \qquad \text{(A-4)}$$

$$a' = \rho_u \left(\frac{\rho_b}{\rho_u} - 1\right), \qquad \text{(A-5)}$$

$$b' = 2\rho_u \left(\frac{\rho_b}{\rho_u} - 1\right) A', \qquad \text{(A-6)}$$

$$c' = \rho_u \left(\frac{\rho_b}{\rho_u} - 1\right) A'^2. \qquad \text{(A-7)}$$

Therefore,

$$(\Delta P)_{r_c \to r=0} = \frac{-b' + \sqrt{b'^2 - 4a'c'}}{2a'} = \frac{-2\rho_u\left(\frac{\rho_b}{\rho_u}-1\right)A' + \sqrt{\left[2\rho_u\left(\frac{\rho_b}{\rho_u}-1\right)A'\right]^2 - 4\left[\rho_u\left(\frac{\rho_b}{\rho_u}-1\right)A'\right]^2}}{2\rho_u\left(\frac{\rho_b}{\rho_u}-1\right)} = -A' =$$

$$= -\rho_u \left(\frac{2\,SN\,V_z}{1+SN}\right)^2 \left[1 - \frac{1}{\varepsilon_r^2} + \frac{1}{2}\left(1 - \frac{\rho_b}{\rho_u}\right)\frac{k^2}{\varepsilon_r^2}\right], \qquad \text{(A-8)}$$

which is identical to that derived by Ishizuka [17, 22].